inorganics

MDPI

Article

Molecular and Supramolecular Structure of a New Luminescent Hybrid Compound: $(C_5N_2H_{14})_2[BiBr_6]Br{\cdot}H_2O$

Andrey V. Bykov [1], Tatiana A. Shestimerova [1], Mikhail A. Bykov [1], Konstantin A. Lyssenko [1], Vladislav M. Korshunov [2], Mikhail T. Metlin [2], Ilya V. Taydakov [2] and Andrei V. Shevelkov [1,*]

[1] Department of Chemistry, Lomonosov Moscow State University, 119991 Moscow, Russia
[2] P.N. Lebedev Physical Institute of the Russian Academy of Sciences, 119991 Moscow, Russia
* Correspondence: shev@inorg.chem.msu.ru

Abstract: The reaction of homopiperazine, $C_5N_2H_{12}$, with $BiBr_3$ in strong hydrobromic acid affords a new organic-inorganic hybrid $(C_5N_2H_{14})_2[BiBr_6]Br{\cdot}H_2O$. It crystallizes in the orthorhombic space group, *Pbca*, with unit cell dimensions of a = 15.0775 (2), b = 15.7569 (2), and c = 20.7881 (4) Å, and eight formula units per unit cell. The crystal structure features slightly distorted octahedral $BiBr_6^{3-}$ and monoatomic Br^- anions in the inorganic substructure and $C_5N_2H_{14}^{2+}$ dications and adjacent water molecules in the organic substructure. Various weak interactions that include (N)H···Br, (N)H···O, and (O)H···Br hydrogen bonds ensure the assembling of the structural moieties into a 3D supramolecular structure. $(C_5N_2H_{14})_2[BiBr_6]Br{\cdot}H_2O$ shows two emission bands in the photoluminescence spectrum, a rather narrow deep-blue PL at 432 nm, and a broadband red PL centered at 650 nm. Their nature and relations to the crystal structure are discussed in this paper.

Keywords: hybrid organic-inorganic compounds; halometallates; bismuth; crystal structure; supramolecular ensemble; photoluminescence

Citation: Bykov, A.V.; Shestimerova, T.A.; Bykov, M.A.; Lyssenko, K.A.; Korshunov, V.M.; Metlin, M.T.; Taydakov, I.V.; Shevelkov, A.V. Molecular and Supramolecular Structure of a New Luminescent Hybrid Compound: $(C_5N_2H_{14})_2[BiBr_6]Br{\cdot}H_2O$. *Inorganics* **2022**, *10*, 181. https://doi.org/10.3390/inorganics10110181

Academic Editor: Kazuyuki Takahashi

Received: 10 August 2022
Accepted: 18 October 2022
Published: 25 October 2022

1. Introduction

Recent interest in halometallates stems from striving to replace efficient yet toxic haloplumbates as light-harvesting materials for solar cells [1]. Apart from tin, which shows remarkable instability regarding Sn^{2+} halide complexes [2,3], bismuth is deemed as the closest analog of lead because of the similarity of $6s^2$ cations to Pb^{2+} and Bi^{3+}. Consequently, a search for halobismuthates as potential photovoltaic materials has been launched; however, only 5% photovoltaic efficiency has been achieved so far [4–6]. At the same time, as hundreds of all-inorganic and hybrid halobismuthates have been discovered and studied, the new roles of these compounds emerge. Quite a number of halobismuthates have demonstrated intriguing properties, including photoluminescence [7–12], thermochromism [13–15], piezo- and ferroelectricity [16–18], and nonlinear optical activity [19,20], to name just a few. Consequently, more research into halobismuthates is now oriented towards other properties than light harvesting.

Bismuth forms many halide complexes in the oxidation state of +3. Apart from a number of subvalent cluster compounds [21–23] and Bi^{5+} fluorocomplexes [24,25], the +3 oxidation state is dominant in bismuth halide derivatives. Although halobismuthates (III) are numerous, almost all of them contain a BiX_6^{3-} anion (X = Cl, Br, or I) as a primary building unit. These octahedra share vertices, edges, or faces to form a variety of anions ranging from 0D to 2D [26,27]. Surprisingly, those cases where single BiX_6^{3-} anions do not combine into more complex structures are rare compared to other halometallate anions [28–35]. As a rule, such compounds form with large organic or inorganic cations and demonstrate high reactivity towards moisture. Their isolation is sometimes difficult because even if a starting solution contains a BiX_6^{3-} anion, in a resulting solid, such octahedral anions join to form various bioctahedral units, chains, or layers [36]. Obviously,

the anionic structure of such compounds is sensitive to cations, which serve as templates. Recently, we have shown that homopiperazine, $C_5N_2H_{12}$, can govern the iodobismuthate anionic substructure of organic-inorganic hybrids by utilizing four hydrogen bonds, with two at each nitrogen atom of a cyclic diamine [37]. Moreover, due to the asymmetry of homopiperazine, the crystal structures are free from rotational/positional disorder and can be analyzed in terms of the influence of weak interactions on the overall stability of a hybrid compound.

In this paper, we present a new hybrid compound, $(C_5N_2H_{14})_2[BiBr_6]Br{\cdot}H_2O$, that contains stand-alone $BiBr_6^{3-}$ octahedral and monoatomic Br^- anions assembled into a 3D array by numerous weak interactions generated by homopiperazinum dications serving as templates. We discuss its crystal structure and optical properties, paying special attention to photoluminescent properties and their relations to the crystal structure.

2. Results and Discussion

A facile reaction of homopiperazine with $BiBr_3$ in concentrated hydrobromic acid yields light-yellow crystals of $(C_5N_2H_{14})_2[BiBr_6]Br{\cdot}H_2O$, which can be easily collected upon filtration. The phase identity and purity were confirmed by comparing the X-ray diffraction pattern taken on a finely crushed powder sample, calculated from the crystal data (Figure S1). The resulting solid is stable in air and can be stored in a closed vial. Upon heating, it starts to decompose near 60 °C, releasing a water molecule. The second step of decomposition starts at 240 °C, leading to the destruction and evaporation of the decomposition products (Figure S2).

The crystal structure of $(C_5N_2H_{14})_2[BiBr_6]Br{\cdot}H_2O$ (Figure 1) consists of the inorganic anionic part comprised of $BiBr_6^{3-}$ and Br^- anions, with the $C_5N_2H_{14}^{2+}$ dications and adjacent water molecules forming the organic part. The $BiBr_6^{3-}$ octahedron shows a slight distortion; there are three shorter bonds in the range of 2.78–2.81 Å and three longer bonds at 2.85, 2.91, and 3.01 Å (Table 1). The distortion is not severe and is less pronounced than in mononuclear bromobismuthates with organic cations [32,38,39]. However, comparisons between all-inorganic bromobismuthates and small organic cations [40] show that the latter feature almost undistorted $BiBr_6^{3-}$ anions; for instance, the range of Bi-Br bond distances in Cs_3BiBr_6 is very narrow: 2.83–2.85 Å [28]. This confirms that the $6s^2$ lone pair on the Bi atom does not display stereochemical activity, which is normal unless very electronegative ligands like fluorine are present [41]. The distance between the bromine atoms of $BiBr_6^{3-}$ octahedra exceeds twice the van der-Waals radius of bromine [42,43]; besides, the bromine atoms of the octahedra and separate Br^- anions do not interact. Therefore, the inorganic substructure can be described as stand-alone $BiBr_6^{3-}$ and Br^- anions present in a 1:1 ratio.

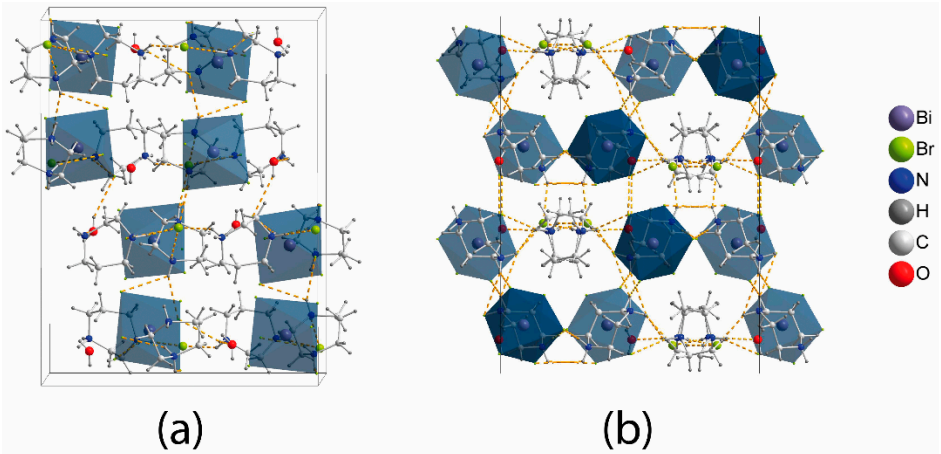

Figure 1. Crystal structure of $(C_5N_2H_{14})_2[BiBr_6]Br{\cdot}H_2O$: (**a**) view slightly off the a-axis and (**b**) projection onto the (010) plane.

Table 1. Selected interatomic distances and angles in the $BiBr_6^{3-}$ anion in the crystal structures of $(C_5N_2H_{14})_2[BiBr_6]Br{\cdot}H_2O$.

Atoms	Distance, Å	Atoms	Angle, °
Bi1–Br1	2.8057(4)	Br1—Bi1—Br4	173.576(13)
Bi1–Br2	2.9063(4)	Br2—Bi1—Br6	177.504(13)
Bi1–Br3	3.0119(4)	Br3—Bi1—Br5	175.040(13)
Bi1–Br4	2.7977(4)		
Bi1–Br5	2.7785(4)		
Bi1–Br6	2.8522(4)		

The $BiBr_6^{3-}$ and Br^- anions form hydrogen bonds with the homopiperazinium cations, $C_5N_2H_{14}^{2+}$, and the water molecules of the organic substructure, thus, composing a 3D supramolecular ensemble. The Br^- anion has a tetrahedral environment of four $C_5N_2H_{14}^{2+}$ cations (Figure 2) with relatively short (N)H···Br distances, ranging from 2.41 to 2.69 Å. The tetrahedral arrangement of these hydrogen bonds is more typical for Cl^- anions [31].

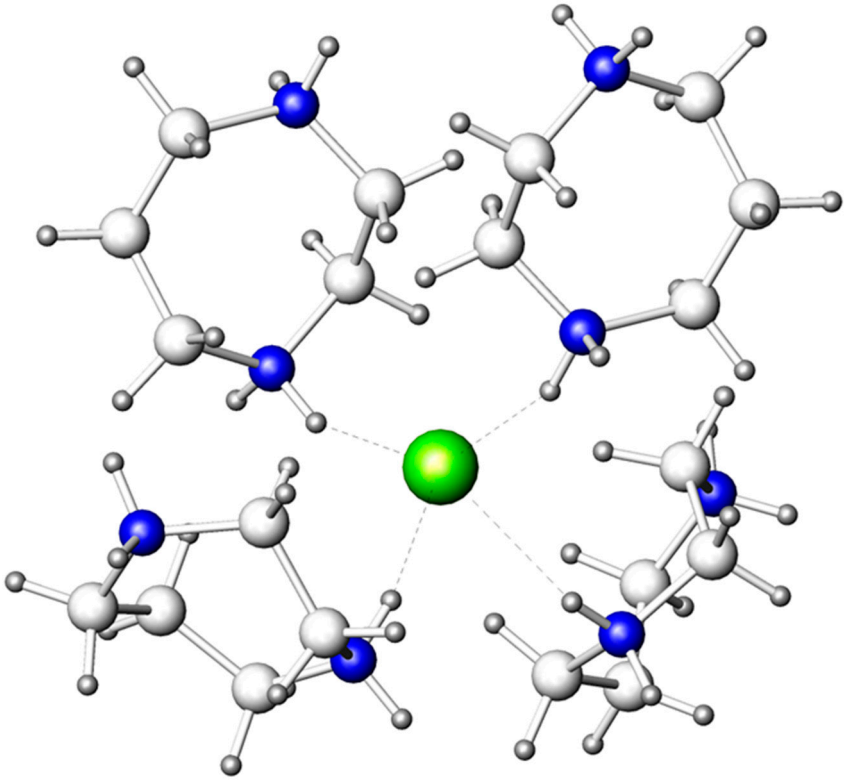

Figure 2. Arrangement of four $C_5N_2H_{14}^{2+}$ cations around the Br^- anion. Bromine: olive; nitrogen: blue; carbon: light grey; hydrogen: dark grey. (N)H···Br bonds are marked by dashed lines.

There are two independent homopiperazinium cations in the crystal structure. They utilize each nitrogen atom as a donor for making hydrogen bonds (Figure 3). In the first cation containing the N1 and N2 atoms, only the (N)H···Br bonds form from 2.41 to 2.86 Å (Table 2). The second cation, based on the N3 and N4 atoms, has the same kind of (N)H···Br bonds, ranging from 2.41 to 2.69 Å and also form one (N)H···O bond at 1.98 Å with the oxygen atom of the water molecule. Additionally, water has an (O)H···Br hydrogen bond of 2.53 Å with the Br3 atom of the $BiBr_6^{3-}$ anion. Previously, we have shown that homopiperazinium has the propensity to use all hydrogen attached to nitrogen atoms to form hydrogen bonds [37]. This is also observed in $(C_5N_2H_{14})_2[BiBr_6]Br{\cdot}H_2O$; however, the difference is that some hydrogen bonds bifurcate in the title compound, which was not observed previously for this cation.

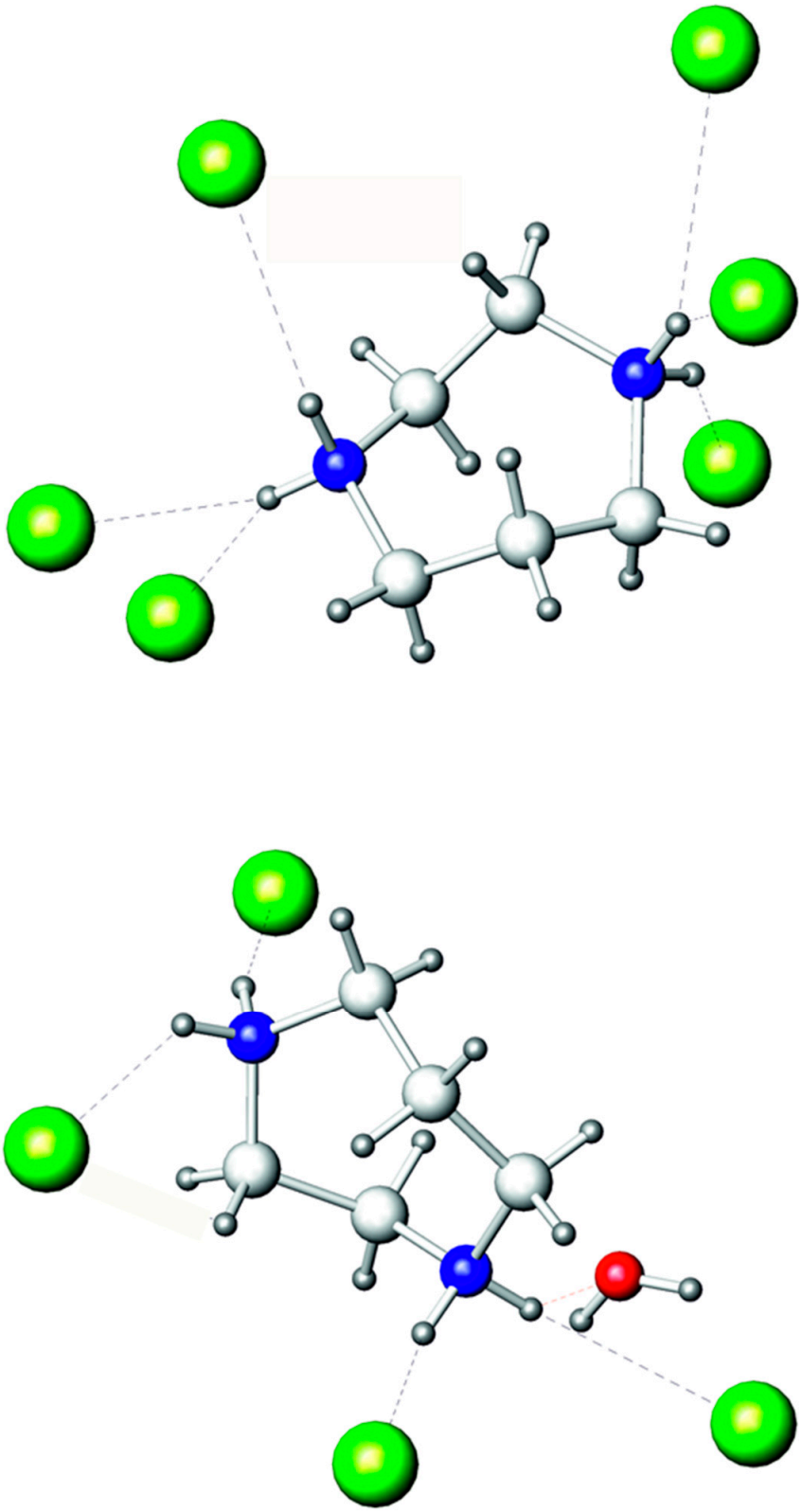

Figure 3. Hydrogen bonds of two independent $C_5N_2H_{14}^{2+}$ cations. Bromine: olive; oxygen: red; nitrogen: blue; carbon: light grey; hydrogen: dark grey. (N)H···Br and (N)H···O bonds are marked by dashed lines.

Table 2. Hydrogen bonding in the crystal structure of $(C_5N_2H_{14})_2[BiBr_6]Br{\cdot}H_2O$.

D–H···A	d (D–H), Å	d (H···A), Å	d(D···A), Å	Angle (D–H···A), °
N1–H1A···Br1	0.91	2.69	3.495 (3)	147
N1–H1B···Br7	0.91	2.41	3.200 (3)	144
N2–H2A···Br7	0.91	2.44	3.267 (3)	151
N2-H2B···Br4	0.91	2.67	3.463 (4)	146
N3-H3C···O1W	0.91	1.98	2.695 (5)	134
N3-H3C···Br7	0.91	2.62	3.448 (4)	151
N4-H4C···Br7	0.91	2.45	3.331 (4)	162
N4-H4D···Br3	0.91	2.53	3.263 (4)	137
OW1-H1WA···Br1	0.85 (4)	2.88 (5)	3.513 (4)	133 (5)
OW1-H1WB···Br3	0.87 (4)	2.53 (4)	3.351 (4)	158 (6)

The network of hydrogen bonds can integrate inorganic and organic substructures into 1D [32], 2D [35], or 3D [44] arrays by quite a few weak interactions [45]. However, covalent bonds do not spread in any direction of the lattice as they are confined to the Bi-Br interactions in the $BiBr_6^{3-}$ anion and the C-C, C-N, C-H, and N-H bonds in the organic cations. In the title compound, a 3D network is formed. Consequently, it is expected that the energy bands in the electronic structure are flat and the band gap is direct [46]. Figure 4 shows the Kubelka–Munk transform of the diffuse reflectance spectrum, which gives a band gap value of 2.96 eV for the direct gap model. For comparison, the indirect gap model gives 2.87 eV. The small difference is not surprising since flat bands are expected; furthermore, both band gap values agree with the light-yellow color of the compound.

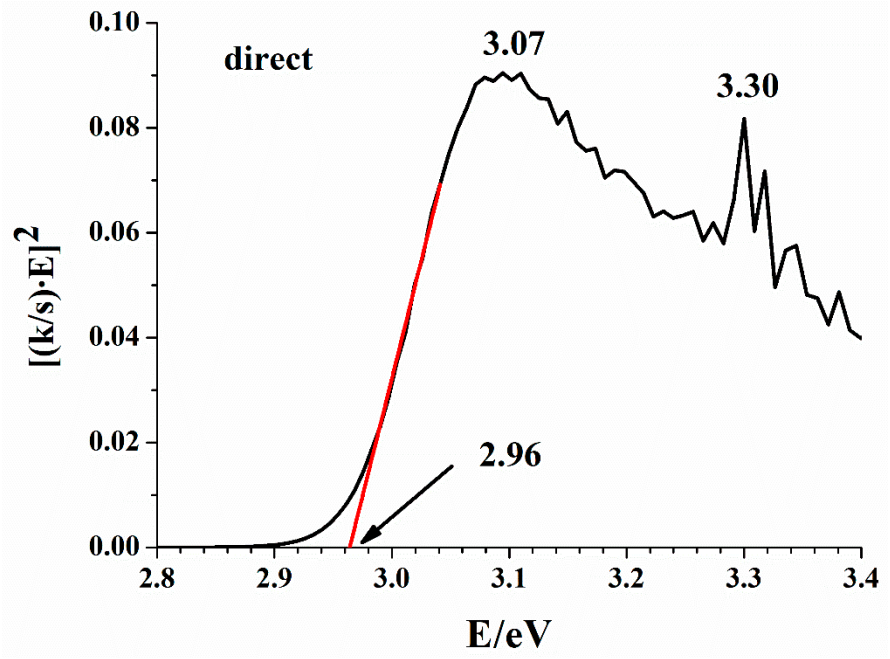

Figure 4. Kubelka–Munk plot for $(C_5N_2H_{14})_2[BiBr_6]Br{\cdot}H_2O$; a direct gap approximation.

The photoluminescent measurements performed at room temperature returned no signal. However, upon excitation at 77 K, two emission bands were recorded, which are shown in Figure 5, together with the respective excitation spectra. The rather narrow band at 432 nm has a full-width half-maximum (FWHM) of 44 nm and a Stokes shift of 0.2 eV. Typically, for bromobismuthates, the charge transfer across the band gap occurs from the 4*p*-states of bromine to the 6*p*-states of bismuth (ligand-to-metal charge transfer, LMCT) [47,48]. Such an LMCT excites an electron across the band gap, leaving a hole at the top of the valence band. The electron and hole can freely move, thus, forming a loosely bound exciton, for which the recombination yields a deep-blue emission with a relatively small Stokes

shift, which can be explained by the defect-free molecular structure of the $BiBr_6^{3-}$ anion. This model is supported by a short exciton lifetime, as can be seen in Figure 6a. We note that such a high-energy emission is observed in bromobismuthates for the first time; to the best of our knowledge, no emission below 469 nm was reported previously [9].

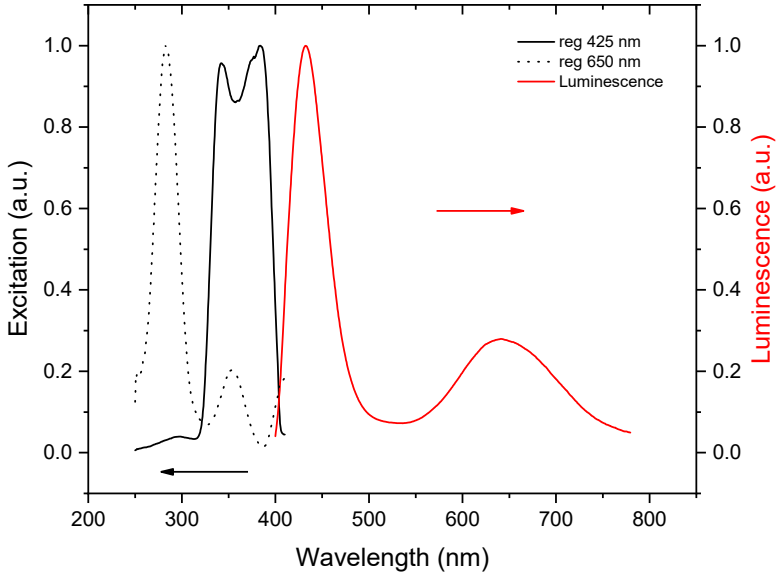

Figure 5. The photoluminescence emission (red) and excitation (black) spectra of $(C_5N_2H_{14})_2[BiBr_6]Br{\cdot}H_2O$ at 77 K.

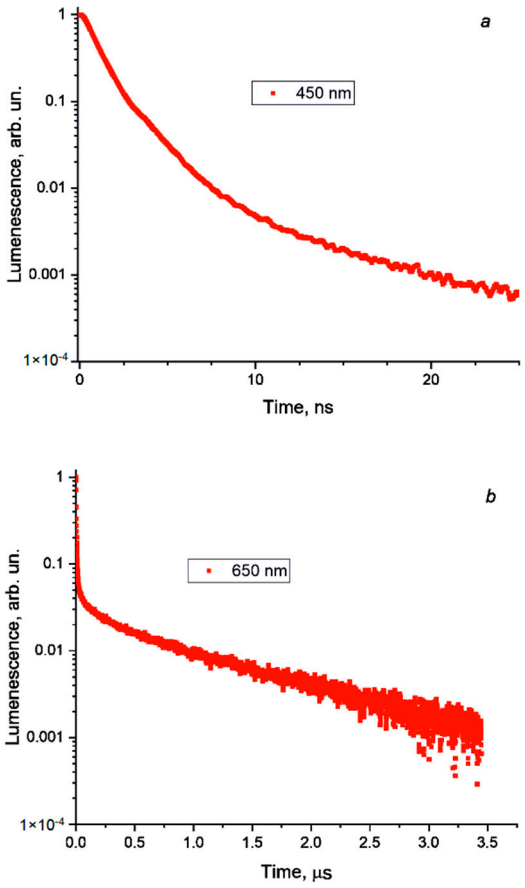

Figure 6. Photoluminescence lifetime for (**a**) deep-blue emission, τ_{ave} = 2.19 ns and (**b**) red emission, τ_{ave} = 0.71 μs.

A broad red emission centered at 645 nm has an FWHM of nearly 110 nm and a large Stokes shift of about 1.4 eV. Remarkably, the excitation bands are blue-shifted with respect to those for the deep-blue emission band, which is seen as an additional peak near 3.3 eV on the Kubelka–Munk plot. We infer that, in this case, the excitation does not involve LMCT but is rather metal-centered (MC). It involves a lower-lying $6s^2$ bismuth lone pair excited to 6*p*-states [49]. Most probably, the local distortions of the $BiBi_6^{3-}$ anions induce small polarons, which trap charge carriers, leading to self-trapped excitons [50–52], and finally, this results in a long exciton lifetime, as is shown in Figure 6b. Given the large Stokes shift, long lifetime, and broad emission band, we attribute the red emission to the $^1S_0 \leftarrow {}^3P_1$ transition, which is spin-forbidden but allowed, owing to strong spin-orbit coupling with the $^1P_1$ state.

3. Materials and Methods

Synthesis. Homopiperazine $C_5N_2H_{12}$ (98%, Acros Organics, Geel, Belgium), $BiBr_3$ (pure, SoyuzReaktiv, Moscow, Russia), and hydrobromic acid HBr (pure for analysis, Reakhim, Staraya Kupavna, Russia) were used as received. A solution of 0.1936 g of $BiBr_3$ in concentrated HBr (1.7 mL) was added to a solution of 0.0867 g of homopiperazine in the same acid (1.3 mL). Lightly-colored yellow crystals precipitated within a day and were filtered off under vacuum and dried in air at room temperature.

Powder X-ray diffraction analysis (PXRD) was performed on an Imaging Plate Guinier Camera (Huber G670, Cu-Kα1 radiation, λ = 1.540598 Å, Rimsting, Germany)). For data collection, crystals were finely crushed in an agate mortar, and the resulting powder was fixed on a holder using scotch tape. The XRD pattern is given in Figure S1.

Thermal analysis. Thermogravimetric analysis was performed (Table S1) using a NETZSCH 209 F1 Libra thermobalance (NETZSCH, Selb, Germany). Samples were heated in alumina crucibles under dry nitrogen flow up to 623 with the ramp rate of 5 K·min^{-1}. The NETZSCH Proteus Thermal Analysis program was used for the data processing. The mass loss at the first stage above 60 °C is 1.98% (-H_2O, 1.82%).

Crystal structure determination. Well-shaped single crystals of the title compound were selected from reaction product. The single crystal diffraction data were measured using a Bruker D8 Quest diffractometer (Bruker, Karlsruhe, Gemany) equipped with a CMOS detector (MoKα, λ = 0.71073 Å, graphite monochromator) at 110 and 300 K [53]. Data were corrected for absorption effects using semiempirical methods implemented in SADABS (2016/2) [54]. The crystal structure was solved by the intrinsic phase methods, which gave the positions of all the bromine and bismuth atoms. Difference Fourier syntheses in Shelxt (SHELXL-2018/3) gave the positions of all the nitrogen, carbon, and oxygen atoms [55]. Additional difference Fourier synthesis gave two peaks near two neighboring carbon atoms with about 2–2.5 electrons. These peaks were stated as carbon atoms and refined; the result can be considered as two conformations of the cation. The conformations ratio in all tested cases stated was near to 75:25. The carbon and nitrogen hydrogen atoms were refined using riding models, whereas the hydrogen atoms of the H_2O molecules were found in the final Fourier synthesis as small peaks near the oxygen atom and further refined using riding models. The crystal structure was refined by anisotropic approximations of the atomic displacement parameters for all atoms except hydrogens. Isotropic atomic displacement parameters were restricted 1.2 times for the carbon and nitrogen hydrogens and 1.5 times for the oxygen hydrogen atoms and their respective parent atom. Experimental and crystallographic information is given in Table 3 and Table S1 for 110 and 300 K, consequently. Further details of the crystal structures may be obtained from the Cambridge Crystallographic Data Centre by quoting the CCDC number 2192630.

Table 3. Crystallographic data for $(C_5N_2H_{14})_2[BiBr_6]Br{\cdot}H_2O$ at 110 K.

Empirical Formula	**$C_{10}H_{30}BiBr_7N_4O$**
Temperature (K)	110 (2)
Crystal system	Orthorhombic
Space group	Pbca
Cell parameter, *a*, *b*, *c* [Å]	15.0775 (2) 15.7569 (2), 20.7881 (4)
Volume [$Å^3$]	4938.73 (13)
Z	8
Density (calculated) [g cm^{-3}]	2.665
Diffractometer	Bruker D8 Quest
Radiation, λ [Å]	MoK\a, 0.71073
Data collection range (°)	2.111–29.998
R_1 [$F_0 > 4\sigma F_0$]	0.0278
wR_2 [$F_0 > 4\sigma F_0$]	0.0513
Goodness-of-fit	1.020

Optical spectroscopy. Optical diffuse reflectance spectra were recorded using a UV-vis spectrometer Perkin-Elmer Lambda 950 (Perkin-Elmer, Waltham, MA, USA) with an attached diffuse reflectance accessory. Measurements were performed at 298 K in the spectral range of 250–1000 nm, with a scanning rate of 2 nm/s using finely ground polycrystalline samples. The data were transformed into absorbance using the Kubelka–Munk method and plotted as $[(k/s){\cdot}h\upsilon]^2$ against hυ, where *k* is the absorption coefficient, *s* is the scattering coefficient, and *h* is the Planck constant [56,57]. Optical band gap, *Eg*, was approximated by extrapolation to $k = 0$.

Photoluminescence excitation and steady-state emission spectra were recorded at room temperature and 77 K with a Horiba-Jobin-Yvon Fluorolog-QM spectrofluorimeter (Paris, France) equipped with a 75 W ArcTune xenon lamp and a Hamamatsu R13456 photomultiplier sensitive in the 200–980 nm emission range. For low-temperature measurements, the samples were placed in a quartz optical cryostat filled with liquid N_2. Luminescence decays were acquired using the same instrument, using a pulsed DeltaLed excitation source (λ = 370 nm) and EZ-time software for data analysis.

4. Conclusions

We have synthesized a new organic-inorganic hybrid: $(C_5N_2H_{14})_2[BiBr_6]Br{\cdot}H_2O$. Its crystal structure contains the inorganic anions, octahedral $BiBr_6^{3-}$, and the monoatomic Br^-, whereas the organic cationic part is composed of the $C_5N_2H_{14}^{2+}$ dications and water molecules. The cationic and anionic parts are linked by a few hydrogen bonds (of various types), (N)H···Br, (O)H···Br, and (N)H···O, mainly executed by the $C_5N_2H_{14}^{2+}$ cation, which utilizes all its potential hydrogen donor sites. In this way, the structural moieties are assembled into a 3D array. The title compound exhibits a photoluminescent emission composed of two bands. The deep-blue emission is narrow; it has a small Stokes shift and fast decay and is attributed to exciton recombination across the band gap. The red emission is broad, with a large Stokes shift and a long lifetime; it is assigned to the radiative recombination of the self-trapped excitons, appearing due to the local distortions of the $BiBr_6^{3-}$ anions induced by the excitation of the bismuth $6s^2$ lone pair.

Supplementary Materials: The following supporting information can be downloaded at: https://www.mdpi.com/article/10.3390/inorganics10110181/s1, Figure S1. X-ray powder diffraction pattern for (C5N2H14)2[BiBr6]Br·H2O. Experimental profile, blue; calculated from the crystal data, magenta (both measured at 300 K); Table S1. Crystallographic data for (C5N2H14)2[BiBr6]Br·H2O at 300 K; Figure S2. Thermal analysis data for $(C_5N_2H_{14})_2[BiBr_6]Br{\cdot}H_2O$.

Author Contributions: Conceptualization: T.A.S. and A.V.S.; methodology: A.V.B.; formal analysis: K.A.L. and I.V.T.; investigation: A.V.B., M.A.B., V.M.K., and M.T.M.; writing—original draft preparation: T.A.S. and A.V.S.; writing—review and editing: K.A.L., I.V.T. and A.V.S.; supervision: A.V.S.;

project administration: A.V.S.; funding acquisition: A.V.S. All authors have read and agreed to the published version of the manuscript.

Funding: This research was funded by the Russian Foundation for Basic Research, grant number 20-03-00280. The X-ray study was supported by the Lomonosov Moscow State University Program of Development.

Data Availability Statement: CCDC 2192630 contains the supplementary crystallographic data for this paper. These data can be obtained free of charge from The Cambridge Crystallographic Data Centre via www.ccdc.cam.ac.uk/structures, accessed on 8 August 2022.

Acknowledgments: We thank A.V. Grigorieva for assisting with the diffuse reflectance spectroscopy measurements.

Conflicts of Interest: The authors declare no conflict of interest.

References

1. Leong, W.L.; Ooi, Z.E.; Sabba, D.; Yi, C.Y.; Zakeeruddin, S.M.; Graetzel, M.; Gordon, J.M.; Katz, E.A.; Mathews, N. Identifying Fundamental Limitations in Halide Perovskite Solar Cells. *Adv. Mater.* **2016**, *28*, 2439–2445. [CrossRef]
2. Dimesso, L.; Stöhr, M.; Das, C.; Mayer, T.; Jaegermann, W. Investigation on the properties of hybrid $CH_3NH_3Sn_xI_3$ ($0.9 \leq x \leq 1.4$) perovskite systems. *J. Mater. Res.* **2017**, *32*, 4132–4141. [CrossRef]
3. Zhu, Z.; Chueh, C.-C.; Li, N.; Mao, C.; Jen, A.K.-Y. Realizing Efficient Lead-Free Formamidinium Tin Triiodide Perovskite Solar Cells via a Sequential Deposition Route. *Adv. Mater.* **2018**, *30*, 1703800. [CrossRef] [PubMed]
4. Yelovik, N.A.; Mironov, A.V.; Bykov, M.A.; Kuznetsov, A.N.; Grigorieva, A.V.; Wei, Z.; Dikarev, E.V.; Shevelkov, A.V. Iodobismutates Containing One-Dimensional BiI_4^- Anions as Prospective Light-Harvesting Materials: Synthesis, Crystal and Electronic Structure, and Optical Properties. *Inorg. Chem.* **2016**, *55*, 4132–4140. [CrossRef] [PubMed]
5. Zhang, W.; Liu, X.; Li, L.; Sun, Z.; Han, S.; Wu, Z.; Luo, J. Triiodide-induced band-edge reconstruction of a lead-free perovskite-derivative hybrid for strong light absorption. *Chem. Mater.* **2018**, *30*, 4081–4088. [CrossRef]
6. Turkevych, I.; Kazaoui, S.; Shirakawa, N.; Fukuda, N. Potential of $AgBiI_4$ rudorffites for indoor photovoltaic energy harvesters in autonomous environmental nanosensors. *Jap. J. Appl. Phys.* **2021**, *60*, SCCE06. [CrossRef]
7. Kundu, K.; Acharyya, P.; Maji, K.; Sasmal, R.; Agasti, S.S.; Biswas, K. Synthesis and Localized Photoluminescence Blinking of Lead-Free 2D Nanostructures of $Cs_3Bi_2I_6Cl_3$ Perovskite. *Angew. Chem. Int. Ed.* **2020**, *59*, 13093–13100. [CrossRef]
8. Dey, A.; Richter, A.F.; Debnath, T.; Huang, H.; Polavarapu, L.; Feldmann, J. Transfer of Direct to Indirect Bound Excitons by Electron Intervalley Scattering in $Cs_2AgBiBr_6$ Double Perovskite Nanocrystals. *ACS Nano* **2020**, *14*, 5855–5861. [CrossRef]
9. Anyfantis, G.C.; Ioannou, A.; Barkaoui, H.; Abid, Y.; Psycharis, V.; Raptopoulou, C.P.; Mousdis, G.A. Hybrid halobismuthates as prospective light-harvesting materials: Synthesis, crystal, optical properties and electronic structure. *Polyhedron* **2020**, *175*, 114180. [CrossRef]
10. Kotov, V.Y.; Ilyukhin, A.B.; Sadovnikov, A.A.; Birin, K.P.; Simonenko, N.P.; Nguyen, H.T.; Baranchikov, A.E.; Kozyukhin, S.A. Bis(4-cyano-1-pyridino)pentane halobismuthates. Light-harvesting material with an optical band gap of 1.59 eV. *Mend. Commun.* **2017**, *27*, 271–273. [CrossRef]
11. McCall, K.M.; Stoumpos, C.C.; Kostina, S.S.; Kanatzidis, M.G.; Wessels, B.W. Strong Electron−Phonon Coupling and Self-Trapped Excitons in the Defect Halide Perovskites $A_3M_2I_9$ (A = Cs, Rb; M = Bi, Sb). *Chem. Mater.* **2017**, *29*, 4129–4145. [CrossRef]
12. Shestimerova, T.A.; Yelavik, N.A.; Mironov, A.V.; Kuznetsov, A.N.; Bykov, M.A.; Grigorieva, A.V.; Utochnikova, L.S.V.V. From Isolated Anions to Polymer Structures through Linking with I_2: Synthesis, Structure, and Properties of Two Complex Bismuth (III) Iodine Iodides. *Inorg. Chem.* **2018**, *57*, 4077–4087. [CrossRef] [PubMed]
13. Goforth, A.M.; Tershansy, M.A.; Smith, M.D.; Peterson, L., Jr.; Kelley, J.G.; DeBenedetti, W.J.; Zur Loye, H.C. Structural Diversity and Thermochromic Properties of Iodobismuthate Materials Containing d-Metal Coordination Cations: Observation of a High Symmetry $[Bi_3I_{11}]^{2-}$ Anion and of Isolated I^- Anions. *J. Am. Chem. Soc.* **2011**, *133*, 603–612. [CrossRef] [PubMed]
14. Gagor, A.; Weclawik, M.; Bondzior, B.; Jakubas, R. Periodic and incommensurately modulated phases in a (2-methylimidazolium) tetraiodobismuthate (iii) thermochromic organic–inorganic hybrid. *CrystEngComm* **2015**, *27*, 3286–3297. [CrossRef]
15. Hao, P.; Wang, W.; Shen, J.; Fu, Y. Non-transient thermo-/photochromism of iodobismuthate hybrids directed by solvated metal cations. *Dalton Trans.* **2020**, *49*, 1847–1853. [CrossRef] [PubMed]
16. Jakubas, R.; Gągor, A.; Winiarski, M.J.; Ptak, M.; Piecha-Bisiorek, A.; Ciżman, A. Ferroelectricity in Ethylammonium Bismuth-Based Organic−Inorganic Hybrid: $(C_2H_5NH_3)_2[BiBr_5]$. *Inorg. Chem.* **2020**, *59*, 3417–3427. [CrossRef]
17. Zhang, Y.-Z.; Sun, D.-S.; Gao, J.-X.; Hua, X.-N.; Chen, X.-G.; Mei, G.-Q.; Liao, W.-Q. A Semiconducting Organic–Inorganic Hybrid Perovskite-type Non-ferroelectric Piezoelectric with Excellent Piezoelectricity. *Chem. Asian J.* **2019**, *14*, 1028–1033. [CrossRef]
18. Szklarz, P.; Gągor, A.; Jakubas, R.; Zieliński, P.; Piecha-Bisiorek, A.; Jakub Cichos, J.; Karbowiak, M.; Bator, G.; Ciżman, A. Lead-free hybrid ferroelectric material based on formamidine: $[NH_2CHNH_2]_3Bi_2I_9$. *J. Mater. Chem. C* **2019**, *7*, 3003–3014. [CrossRef]
19. Dehnhardt, N.; Axt, M.; Zimmermann, J.; Yang, M.; Mette, G.; Heine, J. Band-Gap Tunable, Chiral Hybrid Metal Halides Displaying Second Harmonic Generation. *Chem. Mater.* **2020**, *32*, 4801–4807. [CrossRef]

20. Benin, B.M.; McCall, K.M.; Wörle, M.; Borgeaud, D.; Vonderach, T.; Sakhatskyi, K.; Yakunin, S.; Günther, D.; Kovalenko, M.V. Lone-Pair-Induced Structural Ordering in the Mixed-Valent 0D Metal-Halides $Rb_{23}Bi^{III}{}_xSb^{III}{}_{7-x}Sb^{V}{}_2Cl_{54}$ ($0 \leq x \leq 7$). *Chem. Mater.* **2021**, *33*, 2408–2419. [CrossRef]
21. Lichtenberger, N.; Massa, W.; Dehnen, S. Polybismuthide Anions as Ligands: The Homoleptic Complex $[(Bi_7)Cd(Bi_7)]^{4-}$ and the Ternary Cluster $[(Bi_6)Zn_3(TlBi_5)]^{4-}$. *Angew. Chem. Int. Ed.* **2019**, *58*, 3222–3226. [CrossRef] [PubMed]
22. Baranov, A.I.; Kloo, L.; Olenev, A.V.; Popovkin, B.A.; Romanenko, A.I.; Shevelkov, A.V. Unique Metallic Wires $_\infty{}^1Ni_8Bi_8S$ in a Novel Quasi-1D Compound. Synthesis, Crystal and Electronic Structure, and Properties of Ni_8Bi_8SI. *J. Am. Chem. Soc.* **2001**, *123*, 12375–12379. [CrossRef] [PubMed]
23. Ahmed, E.; Ruck, M. Homo- and heteroatomic polycations of groups 15 and 16. Recent advances in synthesis and isolation using room temperature ionic liquids. *Coord. Chem. Rev.* **2013**, *23–24*, 2892–2903. [CrossRef]
24. Hebecker, C. Über Alkalihexafluorobismutate (V). *Z. Anorg. Allg. Chem.* **1970**, *376*, 236–244. [CrossRef]
25. Popov, A.I.; Val'kovskii, M.D.; Sukhoverkhov, V.F. The structures of alkaline-earth metal fluoroantimonates (V) and fluorobismuthates (V). *Russ. J. Inorg. Chem.* **1990**, *35*, 1608–1611.
26. Adonin, S.A.; Sokolov, M.N.; Fedin, V.P. Polynuclear halide complexes of Bi (III): From structural diversity to the new properties. *Coord. Chem. Rev.* **2016**, *312*, 1–21. [CrossRef]
27. Mercier, N.; Louvain, N.; Bi, W. Structural diversity and retro-crystal engineering analysis of iodometalate hybrids. *CrystEngComm* **2009**, *11*, 720–734. [CrossRef]
28. Chang, J.-H.; Wang, Y.; Doert, T.; Ruck, M. The Polymorphic Nature of M_3BiBr_6 Halides (M = Cs, Rb) and their Reversible Intercalation with Water to Isomorphous Hydrates at Room Temperature. *Z. Anorg. Allg. Chem.* **2021**, *647*, 478–484. [CrossRef]
29. Yelovik, N.A.; Shestimerova, T.A.; Bykov, M.A.; Wei, Z.; Dikarev, E.V.; Shevelkov, A.V. Synthesis, structure, and properties of $LnBiI_6{\cdot}13H_2O$ (Ln = La, Nd). *Russ. Chem. Bull. Int. Ed.* **2017**, *66*, 1196–1201. [CrossRef]
30. Zhang, Z.-P.; Feng, Q.-Y.; Wei, Y.-L.; Gao, Z.-Y.; Wang, Z.-W.; Wang, Y.-M. Three Iodobismuthates Hybrids Displaying Mononuclear, Dimer and 1-D Arrangements Templated by 1,4-diazabicyclo[2.2.2]octane Derivatives: Semiconductor and Photocurrent Response Properties. *J. Clust. Sci.* **2018**, *29*, 725–735. [CrossRef]
31. Shestimerova, T.A.; Golubev, N.A.; Grigorieva, A.V.; Bykov, M.A.; Wei, Z.; Dikarev, E.V.; Shevelkov, A.V. Supramolecular organization of the organic-inorganic hybrid $[\{p\text{-}(CH_3)_2NH—C_6H_4—NH_3\}_2Cl]\,[BiI_6]$: Assembly of a three-dimensional structure via covalent and non-covalent interactions. *Russ. Chem. Bull.* **2021**, *70*, 39–46. [CrossRef]
32. Pandey, S.; Nair, A.; Andrews, A.P.; Venugopal, A. 2,6-Diisopropylanilinium Bromobismuthates. *Eur. J. Inorg. Chem.* **2017**, 798–804. [CrossRef]
33. Chaari, N.; Hamdi, B.; Chaabouni, S.; Zouari, F. Synthesis and Crystal Structure of $[NH_3(CH_2)_2NH_3]_2BrBiBr_6{\cdot}H_2O$. *Anal. Sci.* **2007**, *23*, x183–x184. [CrossRef]
34. Kotov, V.Y.; Buikin, P.A.; Simonenko, N.P.; Ilyukhin, A.B. Hybrid bromobismuthates: Synthesis, thermal stability and crystal structure of multicharged 3-ammoniopyridinium derivatives. *J. Mol. Struct.* **2020**, *1221*, 128807. [CrossRef]
35. Samet, A.; Boughzala, H.; Khemakhem, H.; Abid, Y. Synthesis, characterization and non-linear optical properties of Tetrakis (dimethylammonium) Bromide Hexabromobismuthate: $\{[(CH_3)_2NH_2]^+\}_4{\cdot}Br^-{\cdot}[BiBr_6]^{3-}$. *J. Mol. Struct.* **2010**, *984*, 23–29. [CrossRef]
36. Adonin, S.A.; Gorokh, I.D.; Novikov, A.S.; Samsonenko, D.G.; Korolkov, I.V.; Sokolov, M.N.; Fedin, V.P. Bromobismuthates: Cation-induced structural diversity and Hirshfeld surface analysis of cation–anion contacts. *Polyhedron* **2018**, *139*, 282–288. [CrossRef]
37. Shestimerova, T.A.; Mironov, A.V.; Bykov, M.A.; Grigorieva, A.V.; Wei, Z.; Dikarev, E.V.; Shevelkov, A.V. Assembling Polyiodides and Iodobismuthates Using a Template Effect of a Cyclic Diammonium Cation and Formation of a Low-Gap Hybrid Iodobismuthate with High Thermal Stability. *Molecules* **2020**, *25*, 2765. [CrossRef]
38. Adonin, S.A.; Gorokh, I.D.; Samsonenko, D.G.; Korol'kov, I.V.; Sokolov, M.N.; Fedin, V.P. New structural type in the chemistry of bismuth (III) polynuclear halide complexes: Synthesis and crystal structure of $(H_3O)_3(diquat)_6\{[BiBr_5]\}_6[BiBr_6]{\cdot}2H_2O$. *Russ. J. Inorg. Chem.* **2016**, *61*, 958–963. [CrossRef]
39. Essid, M.; Aloui, Z.; Ferretti, V.; Lefebvre, F.; Ben Nasr, C. Crystal structure, vibrational and optical properties of a new Bi (III) halide complex: $[C_6H_{16}N_2]_5Bi_2Br_{10}(BiBr_6)_2{\cdot}2H_2O$. *Inorg. Chim. Acta* **2017**, *466*, 235. [CrossRef]
40. Li, M.; Li, R.K. Two new bismuth thiourea bromides: Crystal structure, growth, and characterization. *Dalton Trans.* **2014**, *43*, 2577–2580. [CrossRef]
41. Kalinchenko, F.B.; Borzenkova, M.P.; Novoselova, A.V. Solid-phase Interaction of Bismuth(III) and Antimony(III) Fluorides with Alkali Metal Fluorides. *Russ. J. Inorg. Chem.* **1983**, *28*, 1336.
42. Chernyshov, I.Y.; Ananyev, I.V.; Pidko, E.A. Revisiting van der Waals Radii: From Comprehensive Structural Analysis to Knowledge-Based Classification of Interatomic Contacts. *ChemPhysChem* **2020**, *21*, 370–376. [CrossRef] [PubMed]
43. Alvarez, S. A cartography of the van der Waals territories. *Dalton Trans.* **2013**, *42*, 8617–8636. [CrossRef] [PubMed]
44. Buikin, P.A.; Ilyukhin, A.B.; Laurinavichyute, V.K.; Kotov, V.Y. Methylviologen Bromobismuthates. *Russ. J. Inorg. Chem.* **2021**, *66*, 133–138. [CrossRef]
45. Shestimerova, T.A.; Shevelkov, A.V. Metal-inorganic frameworks with pnictogen linkers. *Russ. Chem. Rev.* **2018**, *87*, 28–48. [CrossRef]

46. Sharma, M.; Yangui, A.; Whiteside, V.R.; Sellers, I.R.; Han, D.; Chen, S.; Du, M.-H.; Saparov, B. $Rb_4Ag_2BiBr_9$: A Lead-Free Visible Light Absorbing Halide Semiconductor with Improved Stability. *Inorg. Chem.* **2019**, *58*, 4446–4455. [CrossRef] [PubMed]
47. Skorokhod, A.; Mercier, N.; Allain, M.; Manceau, M.; Katan, C.; Kepenekian, M. From Zero- to One-Dimensional, Opportunities and Caveats of Hybrid Iodobismuthates for Optoelectronic Applications. *Inorg. Chem.* **2021**, *60*, 17123–17131. [CrossRef]
48. Ozòrio, M.S.; Oliveira, W.X.C.; Silveira, J.F.R.V.; Nogueira, A.F.; Da Silva, J.L.F. Novel zero-dimensional lead-free bismuth based perovskites: From synthesis to structural and optoelectronic characterization. *Mater. Adv.* **2020**, *1*, 3439–3448. [CrossRef]
49. Tershansy, M.A.; Goforth, A.M.; Gardinier, J.R.; Smith, M.D.; Peterson Jr., L.; zur Loye, H.-C. Solvothermal syntheses, high- and low-temperature crystal structures, and thermochromic behavior of [1,2-diethyl-3,4,5-trimethyl-pyrazolium]$_4$[Bi_4I_{16}] and [1,10-phenanthrolinium][BiI_4]·(H_2O). *Solid State Sci.* **2007**, *9*, 410–420. [CrossRef]
50. Lin, H.; Zhou, C.; Tian, Y.; Siegrist, T.; Ma, B. Low-Dimensional Organometal Halide Perovskites. *ACS Energy Lett.* **2018**, *3*, 54–62. [CrossRef]
51. Zhou, J.; Li, M.; Ning, L.; Zhang, R.; Molokeev, M.; Zhao, J.; Yang, S.; Han, K.; Xia, Z. Broad-Band Emission in a Zero-Dimensional Hybrid Organic [$PbBr_6$] Trimer with Intrinsic Vacancies. *J. Phys. Chem. Lett.* **2019**, *10*, 1337–1341. [CrossRef] [PubMed]
52. Zhoua, G.; Sua, B.; Huanga, J.; Zhang, O.; Xiaa, Z. Broad-band emission in metal halide perovskites: Mechanism, materials, and applications. *Mater. Sci. Eng. R Rep.* **2020**, *141*, 100548. [CrossRef]
53. Bruker Corporation. *SMART (Control) and SAINT (Integration) Software, Version 5.0*; Bruker AXS Inc.: Madison, WI, USA, 1997.
54. Krause, L.; Herbst-Irmer, R.; Sheldrick, G.M.; Stalke, D. Comparison of silver and molybdenum microfocus X-ray sources for single-crystal structure determination. *J. Appl. Cryst.* **2015**, *48*, 3–10. [CrossRef] [PubMed]
55. Sheldrick, G.M. Crystal structure refinement with SHELXL. *Acta Cryst. Sect. C Struct. Chem.* **2015**, *71*, 3–8. [CrossRef]
56. Kubelka, P.; Munk, F. Ein Beitrag zur Optik der Farbanstriche (Contribution to the optic of paint). *Z. Tech. Phys.* **1931**, *12*, 593–601.
57. Fedeli, P.; Gazza, F.; Calestani, D.; Ferro, P.; Besagni, T.; Zappettini, A.; Calestani, G.; Marchi, E.; Ceroni, P.; Mosca, R. Influence of the synthetic procedures on the structural and optical properties of mixed-halide (Br, I) perovskite films. *J. Phys. Chem. C* **2015**, *119*, 21304–21313. [CrossRef]